E3S Web of Conferences **730**, 05023 (2026) https://doi.org/10.1051/e3sconf/202673005023
Soft Soils 2026

Numerical guidance to multi-direction cyclic testing of soft organic clay with the CYC-DoSS device for railway embankments

Konstantinos Chatzis [1*,3], *Stefano* Muraro[1], and *Cristina* Jommi [1,2]

[1] Department of Geoscience and Engineering, Delft University of Technology, Delft, The Netherlands
[2] Dipartimento di Ingegneria Civile e Ambientale, Politecnico di Milano, Milano, Italy
[3] Haskoning, Delft, The Netherlands

Abstract. The subsoil beneath railway embankments experiences multi-directional cyclic loading across a wide frequency range, conditions that remain largely unexplored in the available literature. This paper presents coupled hydromechanical finite element analyses of two representative cross-sections of Dutch railway embankments to characterise the spatial distribution of cyclic stress increments in the underlying soft soil. The results show that the largest cyclic stress amplitudes occur below the embankment centreline, while stress increments normalised to the initial mean effective stress can become significant at the embankment toe and at the ditch. Principal stress rotations are also pronounced at these locations. In all cases, a greater embankment height reduces these effects. Replicating these conditions in the laboratory requires an apparatus capable of independent multi-axial control at high frequencies. Recent modifications to the CYC-DoSS multi-directional shearing device are presented, which enable accurate force measurement at frequencies up to at least 15 Hz. A pilot test on a natural organic clay specimen demonstrates the device capability to impose complex stress paths and multi-frequency cyclic loading. The results also show that pore pressure generation increases as multi-directional shearing is introduced.

1 Introduction

Assessments of railway embankment stability in the Netherlands seem to indicate insufficient safety levels under current guidelines, yet the actual performance of these embankments shows no evident problems in either serviceability or ultimate limit states. This contrast suggests a high level of conservatism in current assumptions and calculation methods. In the western part of the country, most of the railway embankments are founded on soft soil deposits, mainly consisting of soft organic soils. As the Dutch railway operator ProRail aims to expand the network in terms of speed, carrying capacity and train frequency, there is an urgent need to improve the assessment of the response of soft organic soil deposits under increasing cyclic loads, particularly regarding permanent settlements and excess pore pressure development.

While rail-induced vibrations contain frequencies up to 200 Hz, the range between 0.1 and 20 Hz is the most significantly transmitted to the subsoil and is of greatest relevance from an engineering point of view for embankment stability [1]. Despite the practical relevance of this problem, the cyclic behaviour of soft organic clays at frequencies representative of railway traffic remains largely unexplored. Most available experimental studies on cyclic clay behaviour have been conducted at low frequencies, typically below 1 Hz, and under unidirectional loading conditions [2-5]. Furthermore, the influence of multi-directional shearing on the cyclic response of soft organic soils has received limited attention [6], despite field evidence that multi-directional stress variations are significant features of train-induced loading.

Addressing these gaps requires both adequate characterisation of field loading conditions and advanced laboratory testing. Within the framework of the RESET research programme at TU Delft, a coupled hydromechanical finite element model has been developed to identify representative loading conditions for Dutch railway embankments on soft organic clay. In parallel, the CYC-DoSS multi-directional shearing device [7, 8] was developed to replicate complex stress paths and cyclic loading at high frequencies.

This paper presents the numerical analyses used to characterise the field loading conditions, describes recent modifications to the apparatus to improve its high-frequency performance and reports preliminary experimental results demonstrating the device capabilities on a natural organic clay specimen. The findings provide the basis for the ongoing comprehensive experimental campaign aimed at characterising the cyclic behaviour of Dutch organic clays under representative loading conditions.

* Corresponding author: k.chatzis@tudelft.nl

2 Numerical analyses

Coupled hydromechanical finite element analyses were carried out to investigate the spatial distribution of cyclic stress increments induced by train passage in the soft foundation soils beneath railway embankments.

2.1 Model description

The analyses focused on two representative cross-sections along the Delft–Schiedam railway line, differing in sand embankment height (1.5 m for Section 2 and 4.9 m for Section 5), to assess the influence of embankment geometry on the cyclic stresses in the underlying soft soils (Fig. 1). The soil profile consists of a ballast layer, a sand embankment of variable thickness, a 12 m thick soft organic clay layer and deep sand. All soil layers were modelled as linear elastic materials. The simplification is considered appropriate as the objective of these analyses is to characterise the spatial distribution of cyclic stress increments rather than to predict degradation or permanent deformations. Table 1 reports the parameters adopted for each layer.

A three-dimensional model was developed in OpenSees [9] using stabilised H1-P1ssp 8-node brick elements [10] to avoid volumetric locking near the undrained-incompressible limit. The analyses were performed on the DesignSafe platform [11]. The model domain extends 100 m longitudinally, 60 m laterally from the right side of the ditch and 25 m below the organic clay layer. These dimensions were selected after a sensitivity analysis to ensure that boundary effects do not influence the results at the monitoring points. A symmetry plane along the embankment centreline was exploited to reduce computational cost. Viscous damping boundaries following [12] were applied at the lateral faces, with absorbing coefficients calibrated to the primary and shear wave velocities of each layer. Fixed displacements were applied at the bottom boundary. Rayleigh damping was adopted with coefficients $\alpha_R = 1.74$ and $b_R = 1.47 \times 10^{-3}$, targeting the frequency range of interest (0.1–20 Hz).

Table 1. Material properties used in FE analyses.

Layer	Thickness [m]	$\gamma_{dry}/\gamma_{sat}$ [kN/m^3]	V_s [m/s]	ν [-]
Ballast	0.45	18/20	300	0.2
Sand	Var.	18/20	250	0.2
Organic Clay	12	12/12	80	0.3
Deep Sand	25	18/20	200	0.2

Train passage was represented by moving vertical point loads applied at the top of the ballast [13], with triangular load pulses moving sequentially from node to node. A two-coach VIRM train was modelled with a wheel load of 112 kN, inter-axle spacing of 2.5 m within bogies and 17.5 m between bogies. Speeds ranging from 80 to 170 km/h were considered, representative of operating conditions on this railway section. As the results did not differ significantly across the speed range, only the results for 170 km/h are presented hereafter.

The mesh density was selected to ensure a minimum of five elements per shortest wavelength of interest, resulting in a maximum element size of approximately 0.8 m in the organic clay. A sensitivity analysis with the element size refined to 0.4 m showed minimal changes in the computed stress increments at the monitoring points. The node-to-node spacing along the ballast layer at the load application surface was set to 0.25 m after a dedicated sensitivity analysis. The standard Newmark time integration scheme was adopted with parameters $\gamma_N = 0.5$ and $\beta_N = 0.25$. The time step was selected as the minimum of $\Delta x / V_t$ and $T_{min}/10$, where T_{min} is the minimum period of interest corresponding to 20 Hz [14, 15]. A time step of 0.005 s satisfies both criteria at the highest velocity considered. Additional sensitivity analyses on the time step, omitted for brevity, confirmed that results at the monitoring points were not affected by adopting a smaller time step size.

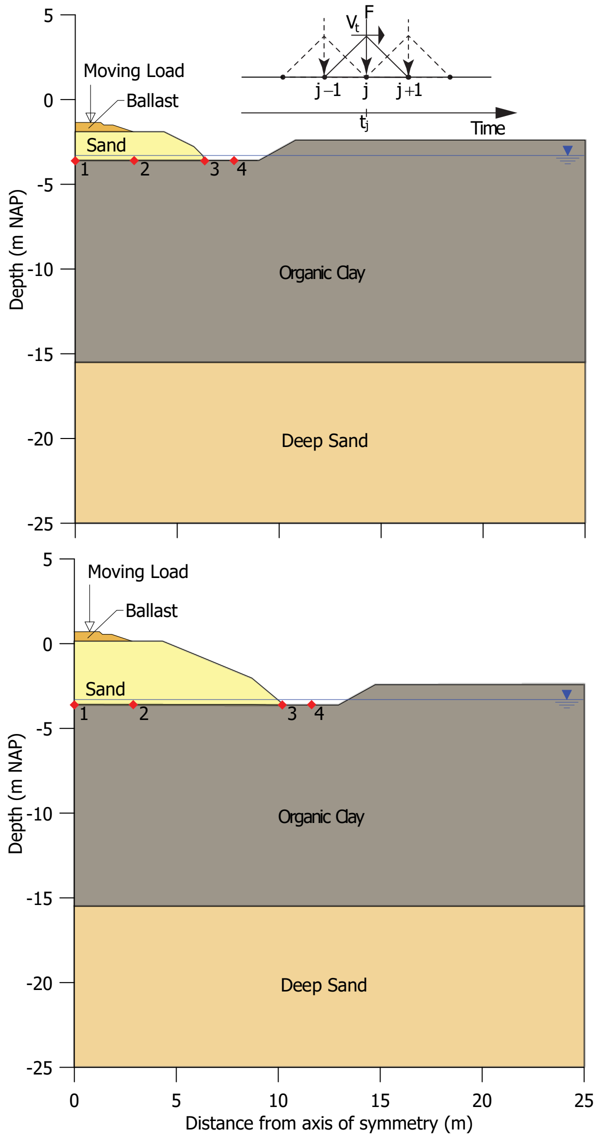

Fig. 1. Representative cross sections along Delft-Schiedam railway line Section 2 (top) and Section 5 (bottom). Reference points under investigation. NAP is the Dutch reference water level.

2.2 Numerical results

Fig. 2 shows the time history of the normalised incremental deviatoric stress $\Delta q/p'_0$ at four monitoring points at the top of the organic clay layer for the two cross-sections. Point 1 is located beneath the embankment centreline, Point 2 under the embankment body, Point 3 at the embankment toe, and Point 4 at the mid-ditch (see Fig. 1).

For Section 5 (Fig. 2a), with the higher embankment, the stress increments are relatively small, with peak values of $\Delta q/p'_0$ remaining below 0.15. For Section 2 (Fig. 2b), with the lower embankment, the cyclic stress amplitudes are significantly larger, reaching peak values of approximately 0.50. In both sections, Point 1 exhibits the highest absolute stress increments. At Points 3 and 4, although the absolute stress amplitudes are smaller, the stress increment normalised to the initial mean effective stress at the bottom of the ditch (Point 4) exceeds that at the embankment toe (Point 3) and, for Section 2, even that of Point 2 beneath the embankment body. Furthermore, the stress signal at these points becomes more complex, with reversals in the sign of the deviatoric stress increment during each bogie passage.

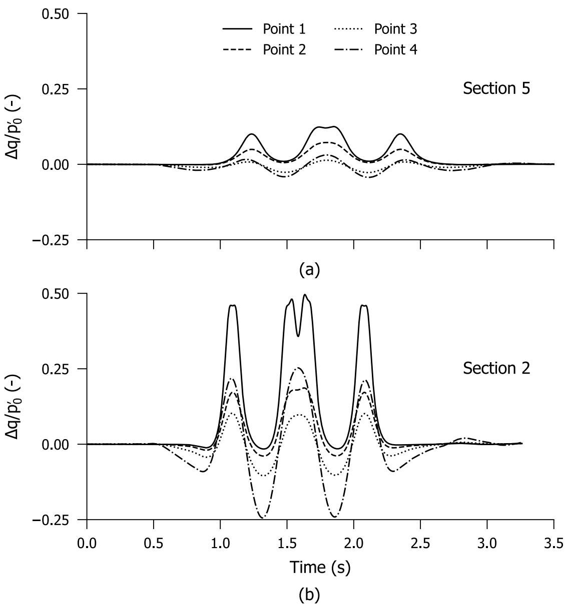

Fig. 2. Normalised incremental deviatoric stress $\boldsymbol{\Delta q/p'_0}$ at four monitoring points for (a) Section 5 and (b) Section 2.

Fig. 3 shows the principal stress rotation during train passage at the top of the organic clay layer, expressed as the rotation angle θ_{yz} of the major principal stress relative to the vertical in the longitudinal plane. For Section 5 (Fig. 3a), with the higher embankment, the principal stress rotation is not significant at most monitoring points, with the exception of Point 3 at the embankment toe where considerable rotation is observed. For Section 2 (Fig. 3b), the reduced embankment height leads to larger principal stress rotation at all points, with the highest rotation occurring at Point 4 at the bottom of the ditch.

These observations correspond to the top of the organic clay layer; at greater depths, both the stress increments and the principal stress rotations diminish. These findings confirm that the largest absolute cyclic stress amplitudes occur beneath the embankment centreline, while stress increments normalised to the initial mean effective stress also become significant at the embankment toe. Principal stress rotations are pronounced at these locations. In all cases, a higher embankment height reduces these effects.

In addition to the spatial complexity of the stress field, the frequency content of the loading is also relevant. Of the broad frequency spectrum generated by railway traffic (up to 200 Hz), the 0.1 to 20 Hz range affects the subsoil response and embankment stability [1].

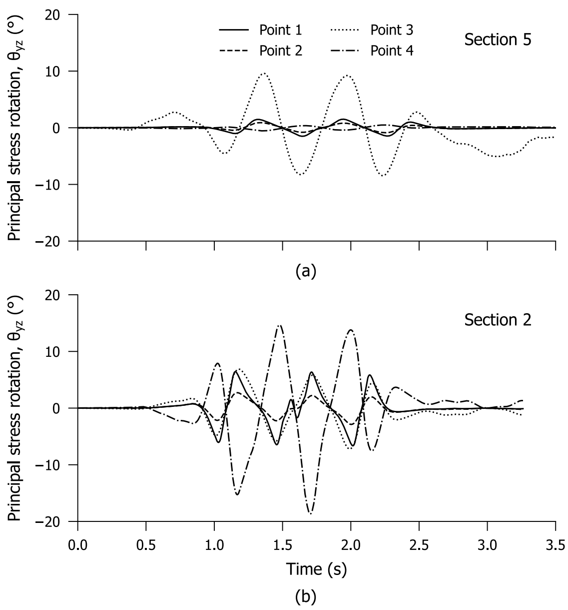

Fig. 3. Principal stress rotation along the longitudinal plane at four monitoring points (a) rotation angle θ_{yz} for Section 5 and (b) rotation angle θ_{yz} for Section 2.

3 Experimental programme

The numerical results presented above are used to inform the development of a new experimental apparatus dedicated to assessing the cyclic behaviour of soft soils for railway infrastructure. Variable frequency range, combined with the stress amplitudes and principal stress rotations identified in the numerical analyses, highlights the need for laboratory testing accounting for multi-directional shearing conditions and at frequencies higher than those typically investigated (1–5 Hz).

The following sections describe the device, the modifications that enable accurate force measurement and a testing programme that probes the device performance and its sensitivity to multi-directional loading, as a first step towards a numerically informed experimental campaign.

3.1 CYC-DoSS device

The tests were performed using the CYC-DoSS device, a cyclic dynamic multi-directional shearing apparatus for the testing of soft soils, developed at TU Delft [7, 8].

The device features three independently controlled hydraulic actuators (x, y, z axes), using servo valves with a 40 L/min flow rate, resulting in a nominal capacity of testing frequencies up to 25 Hz. The load cells have a capacity of 5 kN with an accuracy of ±0.5% at full scale.

Unlike the cyclic triaxial apparatus conventionally used for liquefaction assessment, which applies cyclic loading only on the vertical axis at frequencies typically below 5 Hz, CYC-DoSS actuates three independent axes and operates over a wider frequency range, up to 25 Hz.

Cell pressure is applied through a GDS Pneumatic Controller (GDSPPC). Back pressure and volume are controlled and measured using a GDS Advanced Pressure/Volume Controller (ADVDPC). The independent control of cell pressure and back pressure/volume enables lateral stress to be actively controlled and measured throughout the test, allowing the application of a wide range of stress paths, including K_0 consolidation by enforcing zero average lateral strain. Various local sensors for measuring the displacement field of the specimen (3D Hall effect sensors, laser distance sensors) and fibre optic pore pressure sensors can be mounted. Further details on the apparatus are provided in [7, 8].

3.2 Load cell position modification

It is reported in [8] that the original load cell position caused the measured force signal to include inertial forces from the moving top cap assembly and friction from the linear guideways. At higher testing frequencies, these effects become significant. To address this, the z-axis load cell was relocated from above the top cap assembly to below the bottom cap (see Fig. 4).

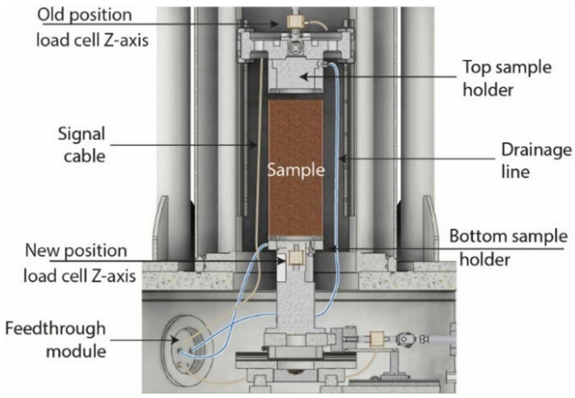

Fig. 4. Sketch of CYC-DoSS with new and old position of Z-axis load (adopted from [7]).

Validation tests were conducted on a dummy rubber specimen with an elastic stiffness comparable to that of a soil specimen, a height of 100 mm and a diameter of 50 mm. Cyclic displacement-controlled tests were performed at 5 Hz with both load cell positions, and at 15 Hz with the new position only.

Fig. 5 shows the measured displacement and force along the z-axis. With the original load cell position (Fig. 5a), the force signal contains parasitic components superimposed on the expected sinusoidal response, and at each reversal of the displacement direction, friction and inertia dominate the force signal. After relocation (Fig. 5b), these effects are largely eliminated and the force at 5 Hz follows the displacement waveform consistently. At 15 Hz (Fig. 5c), both signals remain free of spurious oscillations, demonstrating that the actuators can impose accurate high-frequency cyclic displacements and that the relocated load cell is no longer affected by inertial and frictional artefacts. This improvement is a prerequisite for reliable stress-controlled cyclic tests at higher frequencies, where accurate real-time force feedback governs servo-loop performance.

3.3 Material and testing programme

The tested soil is an organic clay retrieved from the Leendert de Boerspolder site in the Netherlands, which has been extensively characterised in previous studies [16-18]. The specimen was prepared with a height of 100 mm and a diameter of 50 mm. Pore pressure was measured at both the top and bottom of the specimen throughout the test. The present study reports results from a single specimen as a pilot test to demonstrate the apparatus capabilities; a comprehensive investigation is ongoing.

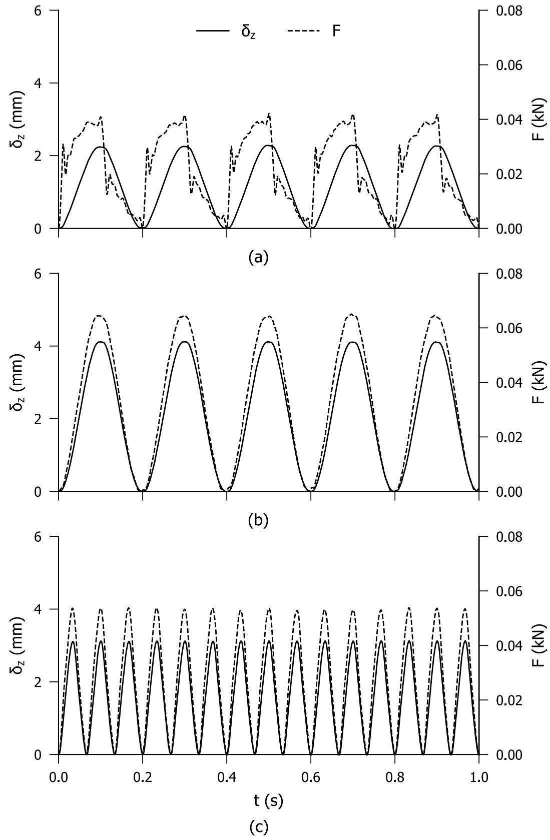

Fig. 5. Measured displacement and load during displacement-controlled tests on dummy rubber specimen (a) at 5 Hz with old load cell position (b), at 5 Hz and (c) 15 Hz with new load cell position.

The specimen was fully saturated by increasing cell pressure and back pressure to 300 and 292 kPa, respectively. The B-value was above 0.98. The specimen was then consolidated under drained K_0 conditions to a mean effective stress of 55 kPa.

A drained stress path was then applied, consisting of drained unloading followed by constant q compression, to probe the versatility of the apparatus. Subsequently, multi-stage undrained cyclic displacement-controlled tests were carried out with a target deviatoric strain amplitude of 1%, a strain level selected to challenge the device at higher frequencies. Displacement control was adopted for this initial validation testing series to ensure stable servo-loop performance across the full frequency range. Stress-controlled tests, enabled by the load cell modification described in Section 3.2, are also planned. Dissipation of excess pore pressures was allowed between stages. The maximum testing frequency was limited to 10 Hz for this first test series on a natural soil specimen, although the validation tests confirmed full reliability of the device up to at least 15 Hz. In Stage 1, multi-frequency tests were performed at 0.1, 1, 5 and 10 Hz for 10 cycles per frequency, with continuous transition between frequencies without interrupting the control. In Stage 2, cyclic loading was applied along the x-axis at 0.1 Hz for 40 cycles. In Stage 3, loading was extended to both horizontal axes (x and y) at 0.1 Hz for 40 cycles. In Stage 4, all three axes (x, y and z) were activated simultaneously at 0.1 Hz for 40 cycles.

3.4 Preliminary results

3.4.1 Stress path control

Fig. 6a shows the applied stress paths in the q–p' plane. The specimen was first consolidated under K_0 conditions, followed by drained unloading and constant q drained compression. The ability of the apparatus to impose such stress paths allows the investigation of the non-monotonic pre-failure response of soft soils from different initial stress states and stress histories, which may influence the subsequent cyclic behaviour. Fig. 6b presents the evolution of K_0 with axial effective stress. The coefficient decreases from approximately 0.85 at low stress levels and converges to an asymptotic value of approximately 0.48, which falls within the range of 0.46–0.50 reported in [18] for the same clay, validating the performance of the apparatus under K_0 conditions.

3.4.2 Cyclic test results

Fig. 7 presents the deviatoric strain time history from Stage 1, where 10 cycles were applied at each of the four frequencies (0.1, 1, 5 and 10 Hz) in continuous succession without interrupting the control. The strain amplitude remains consistent at approximately 1% throughout the full sequence, confirming that the servo-control system maintains the target displacement accurately across the entire frequency range under the same PID (proportional–integral–derivative) settings, a feedback control algorithm that continuously adjusts the actuator command by minimising the error between the measured and target displacements. The zoomed inset shows that even at 10 Hz, the imposed waveform remains sinusoidal and well controlled.

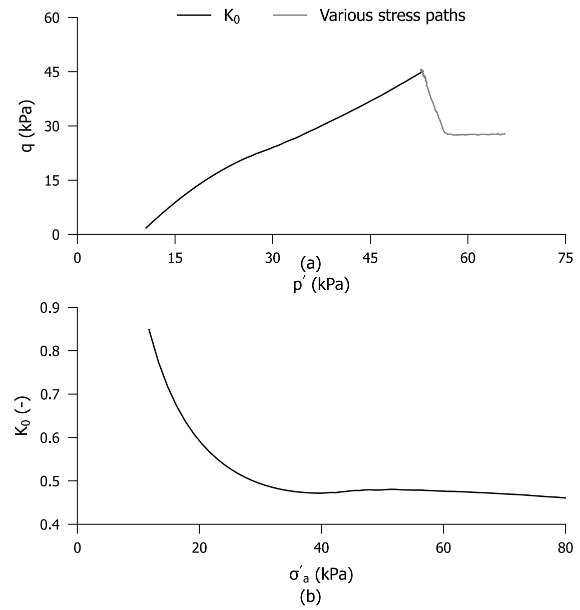

Fig. 6. a) Complex monotonic stress paths and b) evolution of K_0 with axial effective stress during K_0 consolidation.

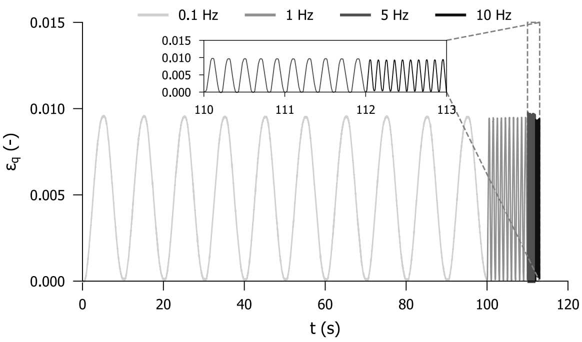

Fig. 7. Measured deviatoric strain time history: 10 cycles at each of four frequencies (0.1, 1, 5 and 10 Hz) on a natural organic clay specimen. Inset: zoomed view at 5 and 10 Hz.

Fig. 8a shows the cyclic deviatoric stress versus deviatoric strain response for all four frequencies. During the initial cycles, the hysteresis loops are wider, indicating higher material damping and more pronounced stiffness degradation. As cycling continues, the loops progressively narrow and stabilise. Across all frequencies, the stiffness increases upon load reversal, and the loops exhibit a concave shape.

Fig. 8b presents the excess pore pressure measured at the top of the specimen versus deviatoric strain. A progressive accumulation of excess pore pressure is observed with an increasing number of cycles. For frequencies up to 5 Hz, the maximum excess pore pressure coincides with the maximum cyclic strain. At 10 Hz, this behaviour reverses, with the maximum excess pore pressure occurring at the minimum cyclic strain. Additionally, at frequencies above 5 Hz, a wider inter-cycle variation of the excess pore pressure is observed, which may be attributed to a non-uniform pore pressure distribution within the specimen at higher loading rates.

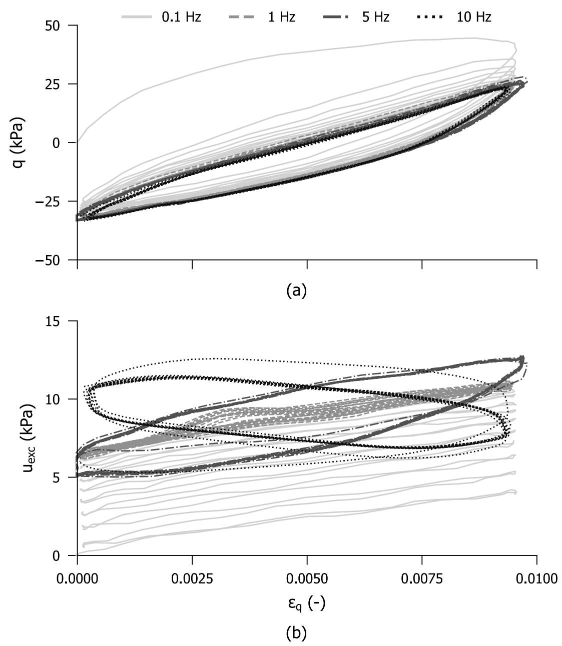

Fig. 8. a) Deviatoric stress vs deviatoric strain and b) Excess pore pressures measured at top of the specimen vs deviatoric strain.

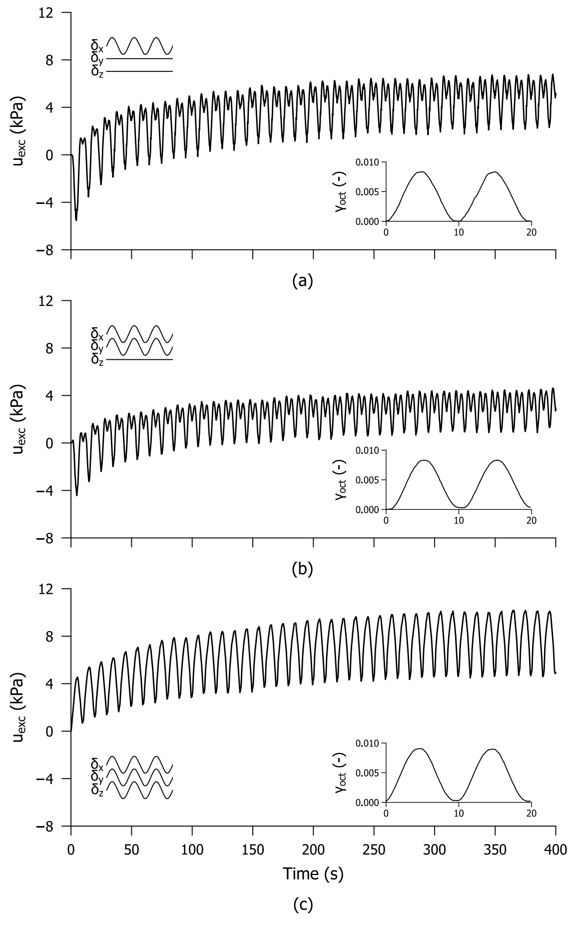

Fig. 9. Excess pore water pressure u_{exc} under (a) unidirectional horizontal, (b) bidirectional horizontal, and (c) combined horizontal and vertical cyclic loading. Insets show the octahedral shear strain γ_{oct} for the first 20 seconds.

Fig. 9 shows the excess pore pressure time histories measured at the top of the specimen under increasingly complex loading configurations: unidirectional horizontal loading along the x-axis (Stage 2, Fig. 9a), bidirectional horizontal loading along x and y (Stage 3, Fig. 9b), and combined horizontal and vertical loading along all three axes (Stage 4, Fig. 9c). The octahedral shear strain amplitude was kept approximately constant across the three stages, as shown in the insets. Despite the comparable octahedral shear strain level, the cyclic pore pressure amplitude increases when the vertical component is added to the shear components. In all three stages, the excess pore pressure accumulates progressively with the number of cycles until an apparent plateau is reached. The differences observed between the three stages underline the importance of investigating the effect of multi-directional loading in more depth, consistent with the field conditions identified in the numerical analyses.

4 Conclusions

This paper presented a combined numerical and experimental study aimed at characterising the cyclic loading conditions beneath railway embankments on soft organic clay and demonstrating the capabilities of the CYC-DoSS multi-directional shearing device for replicating these conditions in the laboratory. The main findings are summarised as follows.

The coupled hydromechanical finite element analyses revealed that the largest absolute cyclic stress amplitudes occur beneath the embankment centreline, while stress increments normalised to the initial mean effective stress become significant at the embankment toe and nearby ditches as well. Principal stress rotations are pronounced at these locations. Higher embankment heights lead to smaller effects in all cases.

Replicating these complex multi-directional loading conditions in the laboratory requires an apparatus capable of independent multi-axial control across a wide frequency range. To this end, targeted modifications were made to the CYC-DoSS multi-directional shearing device. The relocation of the z-axis load cell from above the top cap assembly to below the bottom cap effectively eliminated inertial and frictional artefacts from the force measurement. Validation tests on a dummy specimen confirmed accurate force measurement at frequencies up to at least 15 Hz, enabling future stress-controlled cyclic tests at high frequencies.

The pilot test on a natural organic clay specimen demonstrated that the apparatus is able to impose K_0 consolidation paths with results consistent with previous studies, execute complex monotonic stress paths and maintain accurate displacement control across frequencies from 0.1 to 10 Hz under constant PID settings. The multi-stage cyclic tests showed that pore pressure generation increases with the number of active loading directions, underlining the significance of multi-directional loading conditions.

The present study also identified areas where further development is foreseen. More specifically, the adoption of a multi-axial load cell positioned below the bottom cap or above the top cap would improve the efficiency along the horizontal axes, eliminating inertial and frictional artefacts from the force measurement along these directions as achieved for the vertical axis.

The authors gratefully acknowledge the financial support provided by ProRail under the framework of RESET (Reliable Embankments for Safe Expansion in Rail Traffic). The authors also wish to thank Dr. Chao for his assistance with training and operation of the CYC-DoSS apparatus.

References

1. W. Powrie, L.A. Yang, C.R.I. Clayton, Stress changes in the ground below ballasted railway track during train passage. Proc. Inst. Mech. Eng. Part F J. Rail Rapid Transit **221**, 247–261 (2007). https://doi.org/10.1243/0954409JRRT95
2. M. Li, M. Dai, S. Yao, S. Gao, G. Yuan, Effects of frequencies on the cyclic behavior of marine soft clay under different consolidated stress paths. Mar. Georesour. Geotechnol. **41**, 436–445 (2023). https://doi.org/10.1080/1064119X.2022.2056098
3. J. Huang, J. Hu, H. Wang, J. Chen, S. Liu, Excess pore water pressure behavior of saturated soft clay under cyclic confining pressure with different frequencies. Front. Earth Sci. **10**, 1–15 (2023). https://doi.org/10.3389/feart.2022.1035889
4. L. Guo, J. Chen, J. Wang, Y. Cai, P. Deng, Influences of stress magnitude and loading frequency on cyclic behavior of K0-consolidated marine clay involving principal stress rotation. Soil Dyn. Earthq. Eng. **84**, 94–107 (2016). https://doi.org/10.1016/j.soildyn.2016.01.024
5. M. Zergoun, Y.P. Vaid, Effective stress response of clay to undrained cyclic loading. Can. Geotech. J. **31**, 714–727 (1994)
6. H. Jin, L. Guo, H. Sun, T. Wu, L. Shi, Y. Cai, Energy-based evaluation of undrained cyclic behavior of marine soft clay under multidirectional simple shear stress paths. Acta Geotech. **18**, 2883–2898 (2023). https://doi.org/10.1007/s11440-022-01765-5
7. C. Chao, A comprehensive journey on Dutch organic clays: From element testing through constitutive modelling towards a novel cyclic multidirectional shear device, Ph.D. thesis, Delft University of Technology (2024)
8. C. Chao, W. Broere, C. Jommi, Development of an earthquake simulator for soft soils: Multidirectional Shear Testing Device, in Proceedings of the Journal of Physics: Conference Series, **2647**, 142006 (2024). https://doi.org/10.1088/1742-6596/2647/14/142006
9. F.T. McKenna, Object-oriented finite element programming: frameworks for analysis, algorithms and parallel computing, Ph.D. thesis, University of California, Berkeley (1997)
10. C.R. McGann, P. Arduino, P. Mackenzie-Helnwein, A stabilized single-point finite element formulation for three-dimensional dynamic analysis of saturated soils. Comput. Geotech. **66**, 126–141 (2015). https://doi.org/10.1016/j.compgeo.2014.11.002
11. E.M. Rathje, C. Dawson, J.E. Padgett, J.-P. Pinelli, D. Stanzione, A. Adair, P. Arduino, S.J. Brandenberg, T. Cockerill, C. Dey, M. Esteva, F.L. Haan Jr., M. Hanlon, A. Kareem, L. Lowes, S. Mock, G. Mosqueda, DesignSafe: New cyberinfrastructure for natural hazards engineering. Nat. Hazards Rev. **18**, 06017001 (2017). https://doi.org/10.1061/(ASCE)NH.1527-6996.0000246
12. J. Lysmer, R.L. Kuhlemeyer, Finite dynamic model for infinite media. J. Eng. Mech. Div. **95**, 859–877 (1969)
13. C. Madshus, A.M. Kaynia, High-speed railway lines on soft ground: dynamic behaviour at critical train speed. J. Sound Vib. **231**, 689–701 (2000). https://doi.org/10.1006/jsvi.1999.2647
14. L. Hall, J.-Y. Shih, J.A. Barros, A. Zangeneh, C. Pacoste, J. Johansson, A.M. Kaynia, Design of foundations for high-speed railway embankments: a methodology for setting-up and performing numerical calculations of ground vibrations (SBUF, 2022)
15. V. Galavi, R.B.J. Brinkgreve, Finite element modelling of geotechnical structures subjected to moving loads, in Numerical Methods in Geotechnical Engineering, 235–240 (CRC Press, 2014)
16. C. Jommi, C.Y. Chao, S. Muraro, H.F. Zhao, Developing a constitutive approach for peats from laboratory data. Geomech. Energy Environ. **27**, 100220 (2021). https://doi.org/10.1016/j.gete.2020.100220
17. E. Ponzoni, S. Muraro, A. Nocilla, C. Jommi, Deformational response of a marine silty-clay with varying organic content in the triaxial compression space. Can. Geotech. J. **61**, 1819–1831 (2023). https://doi.org/10.1139/cgj-2023-0058
18. C. Chao, S. Muraro, S., C. Jommi, Improving constitutive modelling of soft organic clays with new experimental insight. Int. J. Numer. Anal. Methods Geomech. **49**, 4480–4501 (2025). https://doi.org/10.1002/nag.70019